# Deep Elastic Strain Engineering of Free-Standing GaN Microbridge

Sufeng Fan,[1,2,3,*] Heyi Wang,[1,*] Chang-Ti Chou,[4,*] Juzheng Chen,[1,5] Ying Han,[2] Jingzhuo Zhou,[1] Xiaocui Li,[2,6] Jyh-Pin Chou,[7,†] Ju Li,[8,‡] and Yang Lu[1,9,§]

[1]*Department of Mechanical Engineering, The University of Hong Kong, Hong Kong, Hong Kong SAR*
[2]*Department of Mechanical Engineering, City University of Hong Kong, Kowloon, Hong Kong SAR*
[3]*School of Mechanics and Safety Engineering, Zhengzhou University, Zhengzhou 450001 China*
[4]*Department of Materials Science and Engineering, Northwestern University, Evanston, Illinois 60208, USA*
[5]*Nano-Manufacturing Laboratory (NML), Shenzhen Research Institute of City University of Hong Kong, Shenzhen 518057, China*
[6]*Department of Materials Science and Engineering, City University of Hong Kong, Kowloon, Hong Kong SAR*
[7]*Graduate School of Advanced Technology, National Taiwan University, Taipei 106319, Taiwan*
[8]*Department of Nuclear Science and Engineering and Department of Materials Science and Engineering, Massachusetts Institute of Technology, Cambridge, Massachusetts 02139, USA*
[9]*Materials Innovation Institute for Life Sciences and Energy (MILES), HKU-SIRI, Shenzhen, China*

(Received 30 August 2025; accepted 2 January 2026; published 23 January 2026)

Gallium nitride (GaN) as a direct band gap semiconductor played a central role in the historical development of efficient blue light-emitting diode and laser diode, in which its intrinsic wide band gap shrinks through the addition of indium (In), thus tuning the color of the light by changing the chemistry. This alloying approach, however, does not allow for dynamic and reversible modulation of the band gap and emission color. Here we show that ultralarge tensile elastic strain can be introduced in microfabricated single crystal GaN microbridges and offer an unprecedented opportunity to modulate its band structure and optoelectronic properties continuously through deep elastic strain engineering. The elastic strain-induced energy band gap modulation was characterized and quantified by *in situ* cathodoluminescence (CL) as well as via strained GaN devices inside a scanning electron microscope. The CL emission of deeply strained (>5%) GaN microbridges has shown substantial band gap reduction from ~3.4 to 2.96 eV (~365 to 420 nm in wavelength), making its optical emission shift from invisible or UV to the blue visible regime. Experimental results agree well with *ab initio* calculation of the change in band gap with increased strain. This dynamic, reversible, and well-controllable strain engineering would facilitate novel device applications in power electronics and optoelectronics.

DOI: 10.1103/x76f-2vj8

Subject Areas: Materials Science, Mechanics, Semiconductor Physics

## I. INTRODUCTION

As an important wide-band-gap semiconductor, gallium nitride (GaN) offers unique characteristics such as high thermal stability, chemical stability, carrier velocity and high breakdown field strength, for applications in high-temperature, high-power, and high-frequency electronics, optics, and laser diodes [1]. In fact, the unique optoelectronic properties, in particular its direct-made GaN the key material in efficient blue light-emitting diode (LED) breakthroughs in the late 1980s and early 1990s, which led to the 2014 Nobel prize in physics [2]. Arguably the most critical step [3] towards achieving the highly efficient blue LED and laser diode in that work is the introduction of indium (In) or aluminum (Al) dopants into wurtzite GaN crystal, so the pristine wide band gap ~3.4 eV in the ultraviolet (UV) regime can be shifted into the visible blue-green light or deep UV regime, thereby enabling color tuning through changing the amount of In/Al in the $(\mathrm{In},\mathrm{Al})_x\mathrm{Ga}_{1-x}\mathrm{N}$ alloys [4–6]. However, with such alloying method [7,8], the band gap and photonic properties, once made, will be fixed and cannot be further modulated dynamically and reversibly. Furthermore, as the $(\mathrm{In},\mathrm{Al})_x\mathrm{Ga}_{1-x}\mathrm{N}$ transistor size shrinks to tens of nanometers and below, the

[*]These authors contributed equally to this work.
[†]Contact author: jpchou@ntu.edu.tw
[‡]Contact author: liju@mit.edu
[§]Contact author: ylu1@hku.hk

discreteness of dopant atoms will eventually come into play, as chemistry can no longer be considered fully continuously tunable as the elastic strain tensor. Here, we demonstrate that elastic strain engineering (ESE) [9] can be an alternative strategy to modulate GaN band gap for optoelectronics applications, such as power transistors and nano- or micro-LED displays [10].

Strain engineering has been a general strategy used in semiconductor manufacturing to improve device performance [11] by modulating the residual elastic strain in the transistor channel to enhance electron mobility, and it is also an effective way to tune and enhance photoelectrical properties of semiconductor nanostructures [9,12]. Judicious choices of epitaxial strain lead to the significant increase of charge-carrier mobility in the complementary metal-oxide-semiconductor (CMOS) technology [11]. Besides, strain also has been used to modulate the electronic band gap and tailor the device characteristics of optoelectronics [12,13]. Recent studies focused on large strain-induced luminescence measurements by photoluminescence (PL) or CL spectroscopy for various semiconductor nanowires because of their enhanced elasticity, for example, strain-induced band gap modulation of ZnO nanowires has been experimentally demonstrated by bending [14] and tensile straining [15]. Apart from direct-band gap semiconductors such as GaAs [16], CdS [17], and CdSe nanowires [18], indirect band gap semiconductors such as micro- or nanoscale germanium [19,20] and diamond [21] were also experimentally studied for their strain effects, for example, Süess *et al.* fabricated germanium microbridges fixed on bulk Si and on silicon on insulator (SOI) substrates with a maximum of 3.1% strain, leading to a band gap shift of 0.21 eV and strongly increased PL intensity [20].

While for GaN as a direct-wide-band gap semiconductor, most previous studies on its strain-modulated electronic and optical properties have been limited to density functional theory (DFT) simulations [22–25], with few experimental works focusing mainly on heterostructure interface or epitaxial-induced strain with small strain values ($\sim 1-3\%$), [11,12,26–29] which are still far from its ideal strain limit [22]. With the enhanced dynamic range of elasticity of materials at micro- or nanoscales [9,30] without inelastic relaxation, there is a huge room for strain engineering GaN [31,32]. So in this work, we investigate the elastic limit and ultrastrength behavior of microfabricated GaN single crystals and explore, both experimentally and computationally, the deep elastic strain engineering (DESE) effect of GaN microbridges under uniaxial tensile loading or unloading at room temperature. We showed that a remarkable band-gap redshift from the invisible range to visible light range (from 3.4 to 2.96 eV) can be achieved by straining the GaN microbridges up to 5.3% along the [0001] axis. Even larger tensile strain close to 7% can be experimentally achieved, suggesting the great potential to use DESE to modulate the optoelectronic properties of GaN for novel device applications.

## II. ACHIEVING ULTRALARGE TENSILE ELASTIC STRAIN IN MICROFABRICATED GAN

To achieve large, uniform elastic deformation, advanced microfabrication of bulk single crystal GaN was

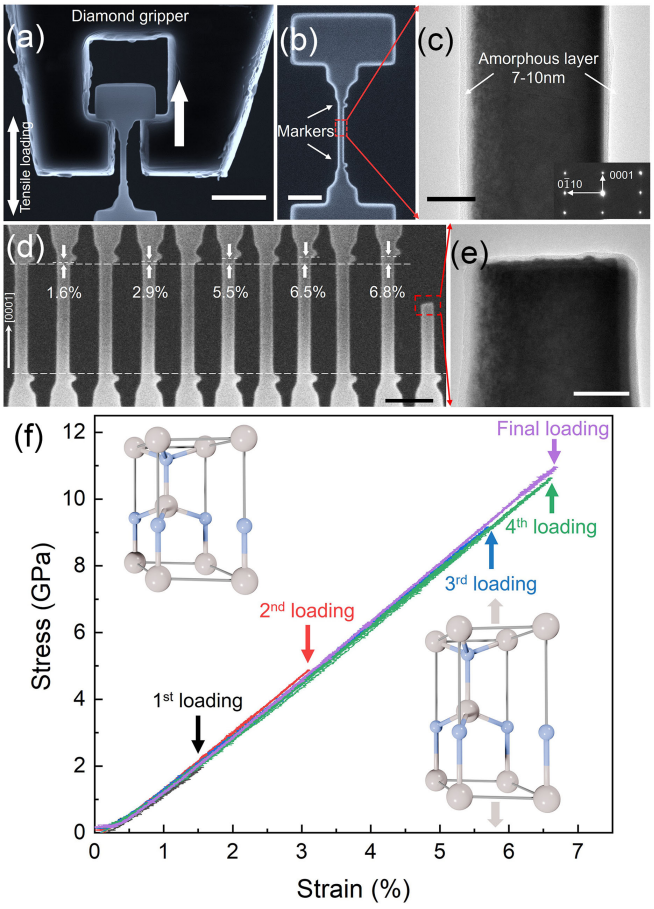


FIG. 1. Microfabrication and deep elastic straining of GaN microbridge. (a) SEM image of a typical as-fabricated GaN microbridge sample and the diamond gripper. Scale bar: 2 μm. (b) The enlarged view of the sample with FIB-deposited fiducial markers serving as the gauge section for measuring the strain value. Scale bar: 1 μm. (c) The surface morphology of the gauge section in TEM, with a thin amorphous layer ($\sim 7-10$ nm). Scale bar: 50 nm. Inset: Selected area electron diffraction (SAED) pattern indicates that GaN tensile sample is a single-crystal hexagonal structure grown along the [0001] orientation. (d) *in situ* loading-unloading tensile tests of a single GaN sample with elastic strain values of ~1.6%, ~2.9%, ~5.5%, ~6.5% are achieved before fracture. The tensile sample finally broke at the fifth cycle with a high strain value of ~6.8%. Scale bar: 500 nm. (e) The morphology of fracture surface in TEM indicated brittle failure. Scale bar: 50 nm. (f) Corresponding stress-strain curves of the multicycle loading-fully unloading test, using different colors to illustrate the data from each cycle. The illustrations of unstrained (left) and strained (right) GaN structures are shown.

performed to produce microbridge-shaped tensile samples [Fig. 1(a)] [21]. These microbridges were focused ion beam (FIB)-sculpted from [0001]-oriented bulk single crystal GaN. Figures 1(b) and 1(c) show the tensile sample up to ~1.2 μm length by ~150 nm width (~200 nm thickness) with well-defined geometry and crystalline orientation (two fiducial markers added by FIB deposition serve for strain measurement). Quantitative *in situ* tensile tests were performed using a Hysitron$^{TM}$ PI 85 PicoIndenter inside a scanning electron microscope (SEM) equipped with a diamond tensile gripper (see Method section) [21].

The sample deformation during straining was video recorded (Supplemental Material movie S1 [33]), and a series of SEM images were extracted from the video of *in situ* tension of a single-crystalline [0001]-oriented GaN microbridge [Fig. 1(d)]. Four complete loading-unloading processes with increasing tensile strain of the microbridge were completed, and the sample completely recovered its original length after strain values of ~1.6%, 2.9%, 5.5%, and 6.5% in each of these cycles, respectively. The corresponding engineering stress-strain curves of loading-fully unloading tests also suggest essentially linear elastic responses [Fig. 1(f)], with an estimated Young's modulus of ~230 GPa, slightly lower than the value of bulk GaN along the same orientation (~295 GPa) [44], possibly due to the surface amorphous layers during microfabrication and growth imperfections [45]. The microbridge eventually fractured when the strain reached an astonishing 6.8%, and the measured tensile strength reached ~11 GPa, showing again the size-induced "ultrastrength" phenomenon [9] that can be exploited for deep strain engineering.

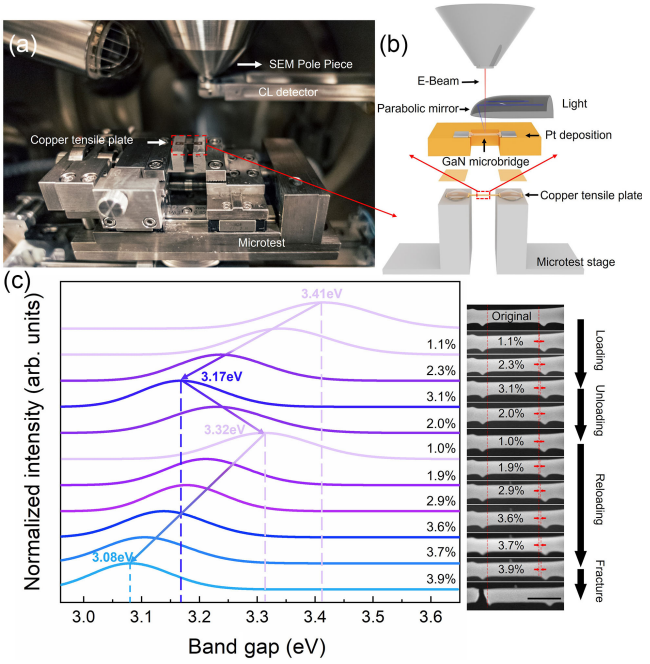


FIG. 2. *in situ* tension-CL analysis on band gap modulation during the GaN loading-unloading process. (a) The *in situ* tension-CL setup, including a microtest tensile stage and a CL detector installed in SEM. (b) The schematic of the measurement setup. The GaN microbridge was fixed on a copper tensile plate which is strained by the tensile stage. (c) The normalized CL spectra shift from invisible to the visible range during the loading-unloading processes, and the corresponding SEM images during loading-unloading processes. Transparent spectra are in the invisible range. Scale bar: 1 μm.

## III. DEEP ELASTIC STRAIN ENGINEERING FOR GAN BAND GAP MODULATION

To investigate and demonstrate how such large, sample-wide elastic strains can substantially affect and modulate the electronic band gap of GaN, an *in situ* tension-CL setup was built inside an SEM, as shown in Fig. 2(a) (see Method section). The microtest tensile machine modulates the sample strain through the control of loading-unloading process of a FIB-fabricated GaN microbridge fixed on a copper tensile specimen, as schematically shown in Fig. 2(b). A series of CL spectra were measured *in situ* for the near band edge (NBE) emission during the loading-unloading process to assess the impact of the uniaxial strain on the electronic energy band gap of GaN along the [0001] direction. The loading-unloading tensile process is recorded by SEM shown in Fig. 2(c), with the tensile strains measured accordingly. The corresponding normalized CL spectra of the GaN microbridge under the uniaxial strains during the loading-unloading process are presented in Fig. 2(c) (the corresponding spectra without normalization are shown in Fig. S1a [33]). As shown in Fig. 2(c), the NBE emission [17,31] of pristine GaN microbridge is 3.41 eV (~364 nm), which is close to the ideal bulk value (~3.4 – 3.42 eV, while size effect on the intrinsic band gap will not impact until below ~10 nm) [46–48]. As shown clearly, the emission peak has a continuous red shift with the increasing tensile strain and the maximum redshift in the loading process is up to 0.25 eV at the tensile strain of 3.1%, with the corresponding emission entering the visible light regime (~380 nm or ~3.26 eV) [49]. During the unloading process, the peak shifts back to 3.32 eV (~373 nm) with the strain reducing to 1.0% after releasing the strain. At the same time, the band gap shifts from visible range to invisible range. Finally, with the tensile strain increasing from 1.0% to 3.9% during the reloading process, the peak shifts from 3.32 to 3.08 eV (~373 to 403 nm in wavelength) into the blue light range, as shown in Fig. 2(c). Compared to the CL spectrum at original state (3.41 eV), there is a huge band gap change of nearly 0.34 eV with 3.9% tensile strain. Each time multiple CL spectra were collected at different positions along the gauge section (by spot-scan CL characterization shown in Fig. S2a [33]) of the stretched sample, and the collected CL spectra appeared consistent (we also verified by area-scan CL characterization shown in Fig. S2b [33]), indicating that the tensile strain is uniformly distributed and can effectively modulate

the electronic properties of GaN microbridges continuously and reversibly (see another case in Fig. S3 [33]).

We further performed *ab initio* DFT calculations to estimate the electronic-band structure evolution upon the corresponding deep tensile straining, as shown in Fig. 3(a) (Supplemental Material movie S2 [33]). GaN has a direct band gap with both conduction band minimum (CBM) and valence band maximum (VBM) located at the Γ point. As shown in Fig. 3(a), CBMs decrease significantly with applied strain, while VBMs are relatively insensitive to strain. Since Ga orbitals dominate CBM, while N orbitals dominate VBM, we conclude that the elastic strain affects the cation-orbital energies more significantly, and we expect this effect to persist for $(\mathrm{In,Al})_x\mathrm{Ga}_{1-x}\mathrm{N}$ alloys as well [23,46]. Figure 3(a) suggests that the band gap would reduce by ∼0.75 eV when the applied strain is 7%, so it would be intriguing to verify the actual band gap reduction under such large elastic strains of GaN microbridges. Figure 3(b) shows the band gap shift from 3.39 to 3.02 eV (∼365 to 410 nm in wavelength) in direct tensile test with the corresponding strain increased from the original state to 4.2%, and an increased intensity trend was observed for spectra without normalization (Fig. S1b [33]; such increasing trend was likewise observed in other cases such as in Fig. S1c, as well as reported in other strained semiconductors [19,20,50–52]).

In our *in situ* CL experiments, the maximum band gap redshift for the tensile strained GaN microbridges was about 0.45 eV (down to 2.96 eV, ∼420 nm in wavelength, fairly close to the typical 430–450 nm wavelength of blue LEDs [3]) with the maximum tensile strain reaching 5.3%. (Fig. S4 [33]) In order to show "strained GaN" for potential device applications, we further designed and microfabricated a strain-fixed GaN device with a push-to-pull structure. As shown in Fig. 3(c), the mechanically strain-fixed GaN device has a thetalike geometry that converts compression loading into tensile straining to stretch the center GaN gauge section [53], with a tensile strain ∼3.1% fixed by FIB clamping of the winglike structures [Figs. 3(d) and 3(e)]. Figure 3(f) shows the strain-fixed GaN microbridge with the band gap redshift from 3.42 to 3.34 eV. Moreover, we can design and microfabricate strained-GaN devices with more complicated geometries for optimal electronic band structure and target figures of merit [54], enabling advanced on-chip photonics and wavelength-tunable optoelectronics [20,55,56] (such as shown in Fig. S5 [33]).

We finally plotted all the experimental and simulation data of the CL emission wavelength of the [0001]-oriented GaN samples against their experimentally achieved tensile strains (Fig. 4). The *in situ* CL experimental data includes the loading-unloading tensile data (solid blue squares in

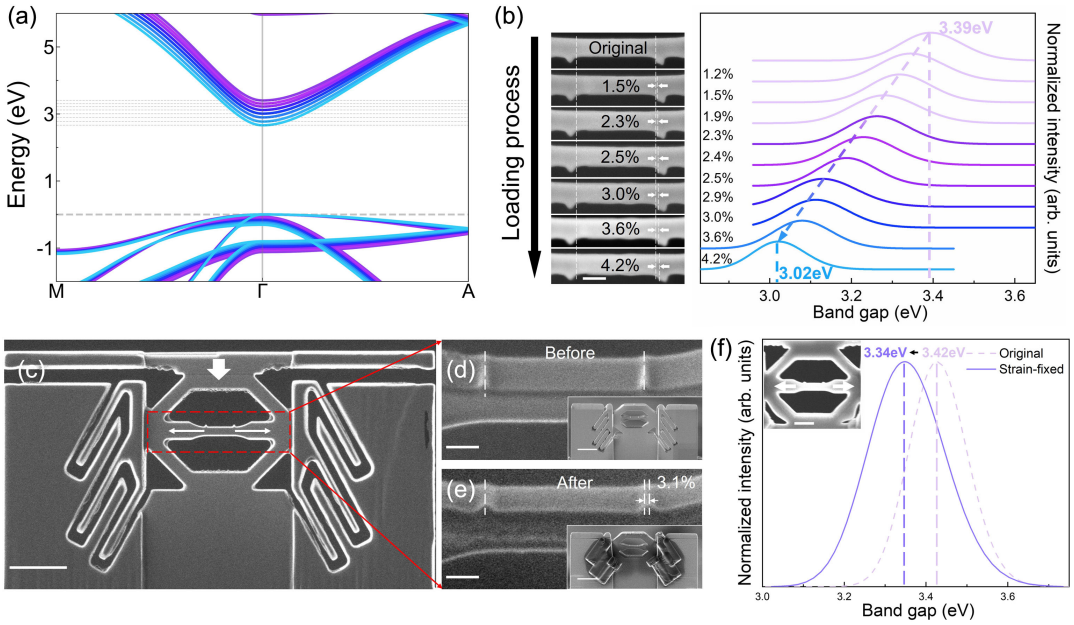


FIG. 3. Deep strain engineering-induced band gap modulation and strain-fixed GaN device. (a) The band structure evolution of GaN as a function of tensile strain from 0% (dark violet) to 7% (light blue) was calculated by DFT. (b) The SEM images of a GaN microbridge during the loading process, and the corresponding normalized CL spectra shift from "invisible UV" (∼3.4 eV) to the "visible blue light" (∼3 eV) regime during the tensile loading process. Initial transparent violet spectra refer to the invisible light regime. Scale bar: 500 nm. (c) The design and working principle of the strain-fixed GaN device with a push-to-pull structure. Scale bar: 2 μm. (d) and (e) The strain-fixed GaN device with 3.1% uniaxial tensile strain. Scale bar: 500 nm. Inset: The morphology of a strain-fixed GaN device before and after strain maintenance. Scale bar: 2 μm. (f) CL characterization of a strain-fixed GaN microbridge with band gap shift from 3.42 to 3.34 eV. Inset: the area where we detected CL characterization. Scale bar: 1 μm.

Fig. 4) and the direct loading data (solid red squares in Fig. 4). It shows the experimental emission data are fairly consistent with the calculation results (hollow gray triangles in Fig. 4), despite a bit discrete due to various experimental factors. As shown in Fig. 4, the original NBE emission of the GaN microbridge is in the UV light range (transparent violet). With increasing tensile strain, the NBE emission gradually enters the visible violet to blue range. The two hollow yellow circles shown in Fig. 4 show the maximum loading-unloading tensile strain and the maximum direct-loading tensile strain (close to 7%) from our uniaxial tensile experiments of GaN microbridges, respectively. As shown in Fig. 4, the maximum tensile strain with the *in situ* CL measurement setup was 5.3%, lower than the uniaxial tensile results. According to the DFT calculations (Fig. 4), if the tensile strain of the GaN microbridge reaches 6.8% [Fig. 1(d)], the corresponding band gap would be further reduced to ~2.68 eV (~463 nm in wavelength), and the corresponding light emitted will be even close to a shade of cyan blue. Our results show that elastic strain is an effective way to substantially modulate the band gap of GaN like chemical alloying and doping, as well as the recently reported intercalation method [57], while being highly reversible and dynamic.

In summary, the tensile straining-induced deep band gap modulation of single crystal GaN microbridges is highly reversible and dynamically tunable over a broad energy range, such as from ~3.41 to 2.96 eV (~365 to 420 nm in wavelength when elastic strain reaching 5.3%), leading to a substantial emission color redshift from invisible UV to visible blue light regime, well comparable to classic chemical alloying method and consistent with our DFT calculations. The deep elastic strain engineering of microfabricated GaN would thus allow for new opportunities in power transistors, optoelectronics, radio frequency components, and laser diodes, [10,58–61] as a significant number of miniaturized devices could be integrated on just one free-standing deep strain-engineered GaN microbridge we have shown here.

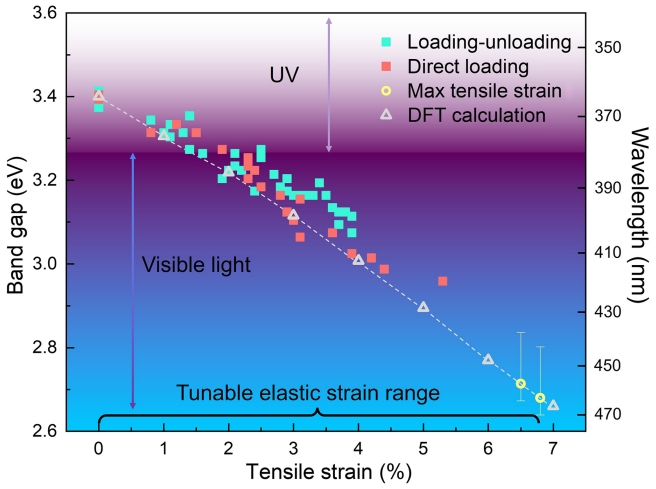


FIG. 4. Summary of the *in situ* CL band gap measurements along with the DFT calculation for [0001]-oriented GaN microbridges upon tensile straining experiments (both loading-unloading and direct tensile loading experiments, respectively). Solid blue squares show the loading-unloading *in situ* CL emission results; solid red squares show the direct tensile loading *in situ* CL emission results; hollow gray triangles refer the DFT calculation results, which agree well with the experimental trend; hollow yellow circles show the maximum tensile strains experimentally achieved in our experiments, with the corresponding band gap and wavelength values estimated by DFT calculations (error bars determined by overall experiment or DFT variances).

## IV. MATERIALS AND METHODS

### A. Microfabrication method

The [0001] oriented single-crystalline bulk GaN was from HELIOS New Materials Co., Ltd. A diamond gripper for the tensile testing was fabricated from a commercially available diamond-tip indenter. The gripper and GaN microbridge samples were both microfabricated by FIB (Scios$^{TM}$ dual-beam system, FEI) operated at 30 kV. The fabrication of GaN microbridges is following the below procedures: at first, a thin lamella was milled from the bulk GaN single crystal by FIB operated with ion beam current 15 nA, and transferred onto a TEM half-grid fixed by Pt deposition; Then the lamella was cut into several specimens and thinning from the top; Lastly, each thin specimen was sculpted into a bridgelike tensile sample, with the surface further polished with only a thin (~6 nm) amorphous layer [as shown in Fig. 1(c)] remaining after FIB machining process.

### B. *In situ* SEM tensile testing

Quantitative tensile tests were performed with a Hysitron$^{TM}$ PI 85 PicoIndenter equipped with a diamond gripper, an *in situ* mechanical measurement setup that enables the tensile process to be observed in a scanning electron microscope (SEM, FEI Quanta$^{TM}$ 450 FESEM) operating at 10 kV. The nominal strain rate was about $1 \times 10^{-3}$ $s^{-1}$ under displacement control. The fracture morphology was observed by a transmission electron microscope (TEM, JEOL 2100F).

### C. *In situ* tension-cathodoluminescence measurement

The *in situ* tension-CL measurement system comprises a micro-tensile stage (Gatan$^{TM}$ Microtest 200) inside the SEM coupled with a CL detector (Gatan$^{TM}$ 450 Monarc system). A copper plate tensile specimen with a slot cut by FIB was fixed on the Microtest loading stages with conductive silver glue, and the GaN microbridge sample was transferred and fixed across the slot of the copper tensile plate by FIB Pt deposition. Then the GaN microbridge was further thinned and polished with a fine FIB beam current of 25 pA at 16 kV. The tensile straining

direction is also along the [0001] orientation. The near band edge (NBE) CL emission spectra were collected in the SEM operated at 10 kV.

### D. DFT calculations for electronic structure

The first-principles calculations are performed using the Vienna *ab initio* simulation package [62,63] with the Heyd-Ernzerhof-Scuseria (HSE) [64] hybrid functional. The fraction of exact exchange in the hybrid-functional calculations is 0.29. The unstrained GaN wurtzite structure is optimized on the HSE level. The lattice constant is 3.192 Å, and c/a ratio is 1.631. When we applied [0001] tensile strain, the Poisson contraction is also considered in our calculations. The energy cutoff of plane wave expansion is 450 eV. The $k$-point sampling in self-consistent field calculation is $8 \times 8 \times 6$.

## ACKNOWLEDGMENTS

This work was supported by Research Grants Council of the Hong Kong Special Administrative Region, China under Project No. RFS2021-1S05 and by National Natural Science Foundation of China under Project No. 12525205. J. P. C. acknowledges the support by The Ministry of Science and Technology in Taiwan (NSTC 113-2112-M-018-003). Y. L. conceived and supervised the research. S. F., H. W., J. C., X. L., Y. H., and J. Z. performed the experimental research. C. T. C. and J. P. C. performed the simulation. S. F., H. W., X. L., and Y. L. analyzed the data. S. F., J. P. C., J. L., and Y. L. co-wrote the initial manuscript. All authors discussed the results and contributed to the final manuscript.

The authors declare no competing financial interests.

## DATA AVAILABILITY

The data are not publicly available. The data are available from the authors upon reasonable request.

[1] S. N. Mohammad, A. A. Salvador, and H. Morkoc, *Emerging gallium nitride based devices*, Proc. IEEE **83**, 1306 (1995), https://www.nobelprize.org/uploads/2018/06/advanced-physicsprize2014.pdf.

[2] T. Bright, *Efficient blue light-emitting diodes leading to bright and energy-saving white light sources*, Sci. Backgr. Nobel Prize Phys, 1 (2014).

[3] S. Nakamura, *Nobel Lecture: Background story of the invention of efficient blue* InGaN *light emitting diodes*, Rev. Mod. Phys. **87**, 1139 (2015).

[4] I. Akasaki, H. Amano, Y. Koide, K. Hiramatsu, and N. Sawaki, *Effects of ain buffer layer on crystallographic structure and on electrical and optical properties of* GaN *and* $Ga_{1-x}Al_xN$ *$(0 < x \leqq 0.4)$ films grown on sapphire substrate by MOVPE*, J. Cryst. Growth **98**, 209 (1989).

[5] S. Nakamura, T. Mukai, M. Senoh, S. i. Nagahama, and N. Iwasa, $In_xGa_{(1-x)}N/In_yGa_{(1-y)}N$ *superlattices grown on* GaN *films*, J. Appl. Phys. **74**, 3911 (1993).

[6] F. Ponce and D. Bour, *Nitride-based semiconductors for blue and green light-emitting devices*, Nature (London) **386**, 351 (1997).

[7] S. F. Chichibu, A. Uedono, T. Onuma, B. A. Haskell, A. Chakraborty, T. Koyama, P. T. Fini, S. Keller, S. P. DenBaars, and J. S. Speck, *Origin of defect-insensitive emission probability in In-containing (*Al, In, Ga*)* N *alloy semiconductors*, Nat. Mater. **5**, 810 (2006).

[8] E. M. Fadaly, A. Dijkstra, J. R. Suckert, D. Ziss, M. A. van Tilburg, C. Mao, Y. Ren, V. T. van Lange, K. Korzun, and S. Kölling, *Direct-bandgap emission from hexagonal* Ge *and* SiGe *alloys*, Nature (London) **580**, 205 (2020).

[9] J. Li, Z. Shan, and E. Ma, *Elastic strain engineering for unprecedented materials properties*, MRS Bull. **39**, 108 (2014).

[10] H. S. Wasisto, J. D. Prades, J. Gülink, and A. Waag, *Beyond solid-state lighting: Miniaturization, hybrid integration, and applications of* GaN *nano-and micro-LEDs*, Appl. Phys. Rev. **6**, 041315 (2019).

[11] S. Bedell, A. Khakifirooz, and D. Sadana, *Strain scaling for CMOS*, MRS Bull. **39**, 131 (2014).

[12] G. Tsutsui, S. Mochizuki, N. Loubet, S. Bedell, and D. Sadana, *Strain engineering in functional materials*, AIP Adv. **9**, 030701 (2019).

[13] M. M. Roberts, L. J. Klein, D. E. Savage, K. A. Slinker, M. Friesen, G. Celler, M. A. Eriksson, and M. G. Lagally, *Elastically relaxed free-standing strained-silicon nanomembranes*, Nat. Mater. **5**, 388 (2006).

[14] K. Watanabe, T. Nagata, Y. Wakayama, T. Sekiguchi, R. Erdélyi, and J. Volk, *Band-gap deformation potential and elasticity limit of semiconductor free-standing nanorods characterized in situ by scanning electron microscope–cathodoluminescence nanospectroscopy*, ACS Nano **9**, 2989 (2015).

[15] B. Wei, K. Zheng, Y. Ji, Y. Zhang, Z. Zhang, and X. Han, *Size-dependent bandgap modulation of* ZnO *nanowires by tensile strain*, Nano Lett. **12**, 4595 (2012).

[16] L. Balaghi, G. Bussone, R. Grifone, R. Hübner, J. Grenzer, M. Ghorbani-Asl, A. V. Krasheninnikov, H. Schneider, M. Helm, and E. Dimakis, *Widely tunable* GaAs *bandgap via strain engineering in core/shell nanowires with large lattice mismatch*, Nat. Commun. **10**, 2793 (2019).

[17] Q. Fu, Z. Y. Zhang, L. Kou, P. Wu, X. Han, X. Zhu, J. Gao, J. Xu, Q. Zhao, and W. Guo, *Linear strain-gradient effect on the energy bandgap in bent* CdS *nanowires*, Nano Res. **4**, 308 (2011).

[18] X. Fu, Z.-M. Liao, Y. Ye, J. Xu, L. Dai, R. Zhu, W. Guo, and D. Yu, *Outermost tensile strain dominated exciton emission in bending* CdSe *nanowires*, Sci. China Mater. **57**, 26 (2014).

[19] J. R. Jain, A. Hryciw, T. M. Baer, D. A. Miller, M. L. Brongersma, and R. T. Howe, *A micromachining-based technology for enhancing germanium light emission via tensile strain*, Nat. Photonics **6**, 398 (2012).

[20] M. J. Süess, R. Geiger, R. Minamisawa, G. Schiefler, J. Frigerio, D. Chrastina, G. Isella, R. Spolenak, J. Faist, and H. Sigg, *Analysis of enhanced light emission from highly*

*strained germanium microbridges*, Nat. Photonics **7**, 466 (2013).
[21] C. Dang, J.-P. Chou, B. Dai, C.-T. Chou, Y. Yang, R. Fan, W. Lin, F. Meng, A. Hu, and J. Zhu, *Achieving large uniform tensile elasticity in microfabricated diamond*, Science **371**, 76 (2021).
[22] L. Dong, S. Yadav, R. Ramprasad, and S. Alpay, *Band gap tuning in* GaN *through equibiaxial in-plane strains*, Appl. Phys. Lett. **96**, 202106 (2010).
[23] Q. Yan, P. Rinke, A. Janotti, M. Scheffler, and C. G. Van de Walle, *Effects of strain on the band structure of group-III nitrides*, Phys. Rev. B **90**, 125118 (2014).
[24] S. Poncé, D. Jena, and F. Giustino, *Hole mobility of strained* GaN *from first principles*, Phys. Rev. B **100**, 085204 (2019).
[25] B. Lim, X. Y. Cui, and S. P. Ringer, *Strain-mediated bandgap engineering of straight and bent semiconductor nanowires*, Phys. Chem. Chem. Phys. **23**, 5407 (2021).
[26] J. H. Son and J.-L. Lee, *Strain engineering for the solution of efficiency droop in* InGaN/GaN *light-emitting diodes*, Opt. Express **18**, 5466 (2010).
[27] I.-W. Feng, J. Li, A. Sedhain, J. Lin, H. Jiang, and J. Zavada, *Enhancing erbium emission by strain engineering in* GaN *heteroepitaxial layers*, Appl. Phys. Lett. **96**, 031908 (2010).
[28] Q. Li and G. T. Wang, *Spatial distribution of defect luminescence in* GaN *nanowires*, Nano Lett. **10**, 1554 (2010).
[29] M. Qi, G. Li, V. Protasenko, P. Zhao, J. Verma, B. Song, S. Ganguly, M. Zhu, Z. Hu, and X. Yan, *Dual optical marker Raman characterization of strained* GaN*-channels on* AlN *using* AlN/GaN/AlN *quantum wells and* $_{15}$N *isotopes*, Appl. Phys. Lett. **106** (2015).
[30] S. Fan, X. Feng, Y. Han, Z. Fan, and Y. Lu, *Nanomechanics of low-dimensional materials for functional applications*, Nanoscale Horiz. **4**, 781 (2019).
[31] X. Fu, H. Nie, Z. Sun, M. Feng, X. Chen, C. Liu, F. Liu, D. Yu, and Z. Liao, *Bending strain effects on the optical and optoelectric properties of* GaN *nanowires*, Nano Res. **15**, 4575 (2022).
[32] H. W. Seo, S. Y. Bae, J. Park, H. Yang, K. S. Park, and S. Kim, *Strained gallium nitride nanowires*, J. Chem. Phys. **116**, 9492 (2002).
[33] See Supplemental Material at http://link.aps.org/supplemental/10.1103/x76f-2vj8 for details on the experimental methods, DFT calculations, and supporting figures, which contains Refs. [28,34–43].
[34] P. Rinke, A. Janotti, M. Scheffler, and C. G. Van de Walle, *Defect formation energies without the band-gap problem: Combining density-functional theory and the GW approach for the silicon self-interstitial*, Phys. Rev. Lett. **102**, 026402 (2009).
[35] A. Rubio, J. L. Corkill, M. L. Cohen, E. L. Shirley, and S. G. Louie, *Quasiparticle band structure of* AlN *and* GaN, Phys. Rev. B **48**, 11810 (1993).
[36] J. Kaczkowski, *Electronic structure of some wurtzite semiconductors: Hybrid functionals vs. ab initio many body calculations*, Acta Phys. Pol. A **121**, 1142 (2012).
[37] M. Grumet, P. Liu, M. Kaltak, J. Klimeš, and G. Kresse, *Beyond the quasiparticle approximation: Fully self-consistent GW calculations*, Phys. Rev. B **98**, 155143 (2018).
[38] Miguel A. Marques, J. Vidal, Micael J. Oliveira, L. Reining, and S. Botti, *Density-based mixing parameter for hybrid functionals*, Phys. Rev. B **83**, 035119 (2011).
[39] Q. Yan, E. Kioupakis, D. Jena, and C. G. Van de Walle, *First-principles study of high-field-related electronic behavior of group-III nitrides*, Phys. Rev. B **90**, 121201(R) (2014).
[40] M. Gajdoš, K. Hummer, G. Kresse, J. Furthmüller, and F. Bechstedt, *Linear optical properties in the projector-augmented wave methodology*, Phys. Rev. B **73**, 045112 (2006).
[41] J. E. Sipe and E. Ghahramani, *Nonlinear optical response of semiconductors in the independent-particle approximation*, Phys. Rev. B **48**, 11705 (1993).
[42] J. Lyons, A. Janotti, and C. Van de Walle, *Carbon impurities and the yellow luminescence in* GaN, Appl. Phys. Lett. **97**, 152108 (2010).
[43] J. Neugebauer and C. G. Van de Walle, *Gallium vacancies and the yellow luminescence in* GaN, Appl. Phys. Lett. **69**, 503 (1996).
[44] R. Nowak, M. Pessa, M. Suganuma, M. Leszczynski, I. Grzegory, S. Porowski, and F. Yoshida, *Elastic and plastic properties of* GaN *determined by nano-indentation of bulk crystal*, Appl. Phys. Lett. **75**, 2070 (1999).
[45] S. Kucheyev, J. Bradby, J. Williams, C. Jagadish, M. Swain, and G. Li, *Deformation behavior of ion-beam-modified* GaN, Appl. Phys. Lett. **78**, 156 (2001).
[46] S. Adachi, *Properties of Semiconductor Alloys: Group-IV, III-V and II-VI Semiconductors* (John Wiley & Sons, New York, 2009).
[47] F. Roccaforte and M. Leszczynski, *Nitride Semiconductor Technology: Power Electronics and Optoelectronic Devices* (John Wiley & Sons, New York, 2020).
[48] D. J. Carter, J. D. Gale, B. Delley, and C. Stampfl, *Geometry and diameter dependence of the electronic and physical properties of* GaN *nanowires from first principles*, Phys. Rev. B **77**, 115349 (2008).
[49] S. Cecie, E. Christine, and S. Lisa, *Biology: Concepts and Applications* (Thomson Brooks, Cole, Belmont, CA, 2005), p. 160.
[50] J. Bruckbauer, P. R. Edwards, S.-L. Sahonta, F. C. Massabuau, M. J. Kappers, C. J. Humphreys, R. A. Oliver, and R. W. Martin, *Cathodoluminescence hyperspectral imaging of trench-like defects in* InGaN/GaN *quantum well structures*, J. Phys. D **47**, 135107 (2014).
[51] S. B. Desai, G. Seol, J. S. Kang, H. Fang, C. Battaglia, R. Kapadia, J. W. Ager, J. Guo, and A. Javey, *Strain-induced indirect to direct bandgap transition in multilayer* $WSe_2$, Nano Lett. **14**, 4592 (2014).
[52] H. Moon, G. Grosso, C. Chakraborty, C. Peng, T. Taniguchi, K. Watanabe, and D. Englund, *Dynamic exciton funneling by local strain control in a monolayer semiconductor*, Nano Lett. **20**, 6791 (2020).
[53] Y. Lu, Y. Ganesan, and J. Lou, *A multi-step method for in situ mechanical characterization of 1-D nanostructures using a novel micromechanical device*, Exp. Mech. **50**, 47 (2010).
[54] Z. Shi, E. Tsymbalov, M. Dao, S. Suresh, A. Shapeev, and J. Li, *Deep elastic strain engineering of bandgap through machine learning*, Proc. Natl. Acad. Sci. U.S.A. **116**, 4117 (2019).

[55] J. Feng, X. Qian, C.-W. Huang, and J. Li, *Strain-engineered artificial atom as a broad-spectrum solar energy funnel*, Nat. Photonics **6**, 866 (2012).

[56] F. Armand Pilon, A. Lyasota, Y.-M. Niquet, V. Reboud, V. Calvo, N. Pauc, J. Widiez, C. Bonzon, J.-M. Hartmann, and A. Chelnokov, *Lasing in strained germanium microbridges*, Nat. Commun. **10**, 2724 (2019).

[57] J. Wang, W. Cai, W. Lu, S. Lu, E. Kano, V. C. Agulto, B. Sarkar, H. Watanabe, N. Ikarashi, and T. Iwamoto, *Observation of 2D-magnesium-intercalated gallium nitride superlattices*, Nature (London) **631**, 67 (2024).

[58] S. Pearton, C. Abernathy, M. Overberg, G. Thaler, A. Onstine, B. Gila, F. Ren, B. Lou, and J. Kim, *New applications advisable for gallium nitride*, Mater. Today **5**, 24 (2002).

[59] Z. Zheng, L. Zhang, W. Song, S. Feng, H. Xu, J. Sun, S. Yang, T. Chen, J. Wei, and K. J. Chen, *Gallium nitride-based complementary logic integrated circuits*, Nat. Electron. **4**, 595 (2021).

[60] S. Kako, C. Santori, K. Hoshino, S. Götzinger, Y. Yamamoto, and Y. Arakawa, *A gallium nitride single-photon source operating at 200 K*, Nat. Mater. **5**, 887 (2006).

[61] Y. Chen, J. Liu, K. Liu, J. Si, Y. Ding, L. Li, T. Lv, J. Liu, and L. Fu, GaN *in different dimensionalities: properties, synthesis, and applications*, Mater. Sci. Eng. R-Rep. **138**, 60 (2019).

[62] G. Kresse and J. Hafner, *Ab initio molecular-dynamics simulation of the liquid-metal–amorphous-semiconductor transition in germanium*, Phys. Rev. B **49**, 14251 (1994).

[63] G. Kresse and J. Furthmüller, *Efficient iterative schemes for ab initio total-energy calculations using a plane-wave basis set*, Phys. Rev. B **54**, 11169 (1996).

[64] J. Heyd, G. E. Scuseria, and M. Ernzerhof, *Hybrid functionals based on a screened Coulomb potential*, J. Chem. Phys. **118**, 8207 (2003).